catalysts

MDPI

Review

In Situ Spectroscopic Studies of Proton Transport in Zeolite Catalysts for NH_3-SCR

Peirong Chen * and Ulrich Simon *

Institute of Inorganic Chemistry and Center for Automotive Catalytic Systems Aachen, RWTH Aachen University, 52074 Aachen, Germany

* Correspondence: peirong.chen@ac.rwth-aachen.de (P.C.); ulrich.simon@ac.rwth-aachen.de (U.S.); Tel.: +49-241-809-9386 (P.C.); +49-241-809-44644 (U.S.)

Academic Editor: Juan J. Bravo-Suarez
Received: 26 October 2016; Accepted: 9 December 2016; Published: 14 December 2016

Abstract: Proton transport is an elementary process in the selective catalytic reduction of nitrogen oxides by ammonia (DeNO$_x$ by NH_3-SCR) using metal-exchanged zeolites as catalysts. This review summarizes recent advancements in the study of proton transport in zeolite catalysts using in situ electrical impedance spectroscopy (IS) under NH_3-SCR reaction conditions. Different factors, such as the metal cation type, metal exchange level, zeolite framework type, or formation of intermediates, were found to influence the proton transport properties of zeolite NH_3-SCR catalysts. A combination of IS with diffuse reflection infrared Fourier transformation spectroscopy in situ (in situ IS-DRIFTS) allowed to achieve a molecular understanding of the proton transport processes. Several mechanistic aspects, such as the NH_3-zeolite interaction, NO-zeolite interaction in the presence of adsorbed NH_3, or formation of NH_4^+ intermediates, have been revealed. These achievements indicate that IS-based in situ methods as complementary tools for conventional techniques (e.g., in situ X-ray absorption spectroscopy) are able to provide new perspectives for the understanding of NH_3-SCR on zeolite catalysts.

Keywords: proton transport; impedance spectroscopy; DRIFTS; reaction mechanism; NO_x emission control; NH_4^+ intermediates

1. Introduction

Selective catalytic reduction (SCR) is one of the key technologies to reduce nitrogen oxide emissions (NO_x) from "lean-burn" engines and power plants [1–3]. Because of their superior activity and hydrothermal stability, Cu- or Fe-exchanged zeolites are widely applied as SCR catalysts, especially in diesel-powered automobiles [3,4]. To meet the continuously tightening NO_x emission legislation, it is necessary to further improve the performance of the metal-exchanged zeolite catalysts in SCR, which requires understanding more deeply both the reaction mechanisms and the real-time physico-chemical properties of the zeolite catalysts under operational conditions [2–6].

For SCR reactions using NH_3 as a reductant (NH_3-SCR; see Equations (1)–(3) for different reaction routes depending on the NO_x composition):

$$4NH_3 + 4NO + O_2 \rightarrow 4N_2 + 6H_2O \text{ (standard SCR)}, \quad (1)$$

$$2NH_3 + NO + NO_2 \rightarrow 2N_2 + 3H_2O \text{ (fast SCR)}, \quad (2)$$

$$8NH_3 + 6NO_2 \rightarrow 7N_2 + 12H_2O \text{ (NO_2 SCR)}. \quad (3)$$

One of the fundamental issues is to understand the NH_3-zeolite interaction. This interaction has been known to largely determine the storage capability, the uptake and release energetics,

and the reactivity of NH_3 within zeolite catalysts [3,7], and eventually the catalytic performance of the zeolite catalysts in NH_3-SCR. Considerable advancements have been achieved by means of, for example, temperature-programmed desorption (TPD), infrared spectroscopy, and X-ray based methods such as Extended X-Ray Absorption Fine Structure, X-ray Absorption Near Edge Structure, X-ray Emission Spectroscopy (all using NH_3 as a probe molecule) [7–13]. Nevertheless, more elementary processes associated with the NH_3 storage and conversion, in particular, the proton transport, are not fully understood.

It is known that proton transport, which can take place either from the bridging hydroxyl groups (Brønsted acid sites) to reactant molecules or between the reaction intermediates, plays an important role in a series of catalytic reactions such as methylation [14], cracking and methanol-to-olefin [15,16], as well as abatement of NO_x emissions [3,4,17]. Comprehensive experimental and theoretical investigations had been performed over zeolites with different framework types (FAU, BEA, MFI, FER, CHA, etc.), in order to understand and take advantage of the proton transport processes for further improving the catalytic performance of zeolites [18–22]. Density functional theory (DFT) calculations revealed that proton transfer takes place in several elementary processes in NH_3-SCR reactions over zeolite catalysts, including NO oxidation, fast SCR, NO_2-SCR, NH_3 oxidation and N_2O decomposition [12,20,22,23]. For Cu-ZSM-5 catalyzed NO decomposition, the presence of protons was found to significantly lower the energy barrier for the NO activation on Cu sites [24]. Although the proton transport processes can be probed by ^1H MAS NMR spectroscopy under well-controlled conditions [12,19,21], studies under technically relevant reaction conditions are practically challenging. In the last years, we applied electrical impedance spectroscopy (IS) to study the proton transport in various zeolites (such as H-ZSM-5, Fe-ZSM-5, Cu-ZSM-5, Cu-SSZ-13, Cu-SAPO-34, etc.) as NH_3-SCR catalysts under in situ or *operando* conditions [17,25–31]. In NH_3-SCR over zeolite catalysts, the adsorption of NH_3 molecules on Brønsted acid sites leads to the formation of ammonium ions (NH_4^+), which interact further with NH_3 molecules forming $NH_4^+ \cdot (NH_3)_n$ complexes at low temperatures [2]. The formed NH_4^+ and $NH_4^+ \cdot (NH_3)_n$ complexes, which can provide additional paths or carriers for proton transport [26,32–34], lead to increased proton conductivities which can be monitored by IS in a broad frequency range (mHz–GHz) [27,32–36]. The consumption of adsorbed NH_3, either by desorption or SCR conversion, leads to decreased conductivity due to a loss of proton carriers [17,26]. A further combination of IS and diffuse reflection infrared Fourier transformation spectroscopy (in situ IS-DRIFTS) allowed us to achieve a molecular understanding of the proton transport processes and their impact in NH_3-SCR catalysis [17,27–29].

In this review, we will briefly introduce the physical background and instrumentation of in situ IS and in situ IS-DRIFTS (Section 2). In Section 3, we will summarize the mechanisms and influential factors of NH_3-supported proton transport in zeolite catalysts, and the impact of proton transport in NH_3-SCR catalysis. The future perspectives, which arise from the achieved understanding, will be discussed at the end (Section 4).

2. Theory and Instruments

2.1. Theory of Impedance Spectroscopy

Impedance spectroscopy is an electric perturbation technique, and can be employed to analyze the mobility of ions in solid materials [37,38]. In a typical IS measurement over zeolite, an alternating voltage $U(\omega)$ with angular frequency ω and amplitude U_0 is applied to form an electric field over a zeolite in thermodynamic equilibrium. A response of the system, i.e., a movement of the mobile cations either via translation motion or a local displacement, is induced by the electric perturbation, and can be macroscopically measured as a current $I(\omega)$. The complex impedance $Z(\omega)$ is defined as

$$Z(\omega) = U(\omega)/I(\omega) \quad (4)$$

and can be described by a real part Z' and an imaginary part Z''. Both depend on the angular frequency ω:

$$Z(\omega) = Z'(\omega) + jZ''(\omega). \quad (5)$$

In the analysis of complex impedance $Z(\omega)$, low-frequency phenomena such as the sample/electrode interface polarization can be identified from the dominating low-frequency tail of the traditional Argand representation (also known as Nyquist plot; the real part Z' is plotted against the imaginary part Z''; see Figure 1a for an example) [39]. The high-frequency processes are more visible in the Modulus plot, which shows the imaginary part of the Modulus M, i.e., $M''(\omega)$, against the frequency f (Figure 1b). The modulus $M''(\omega)$ is defined as

$$M''(\omega) = \omega C_0 Z'(\omega), \quad (6)$$

wherein C_0 is the capacity of the empty capacitor, i.e., the geometric capacitance. Thereby, two distinct relaxation processes, i.e., the local dipolar relaxation (as visualized by the maximum at high-frequency range) and the long-range proton transport (as visualized by the maximum at low-frequency range) can be clearly distinguished in one spectral representation.

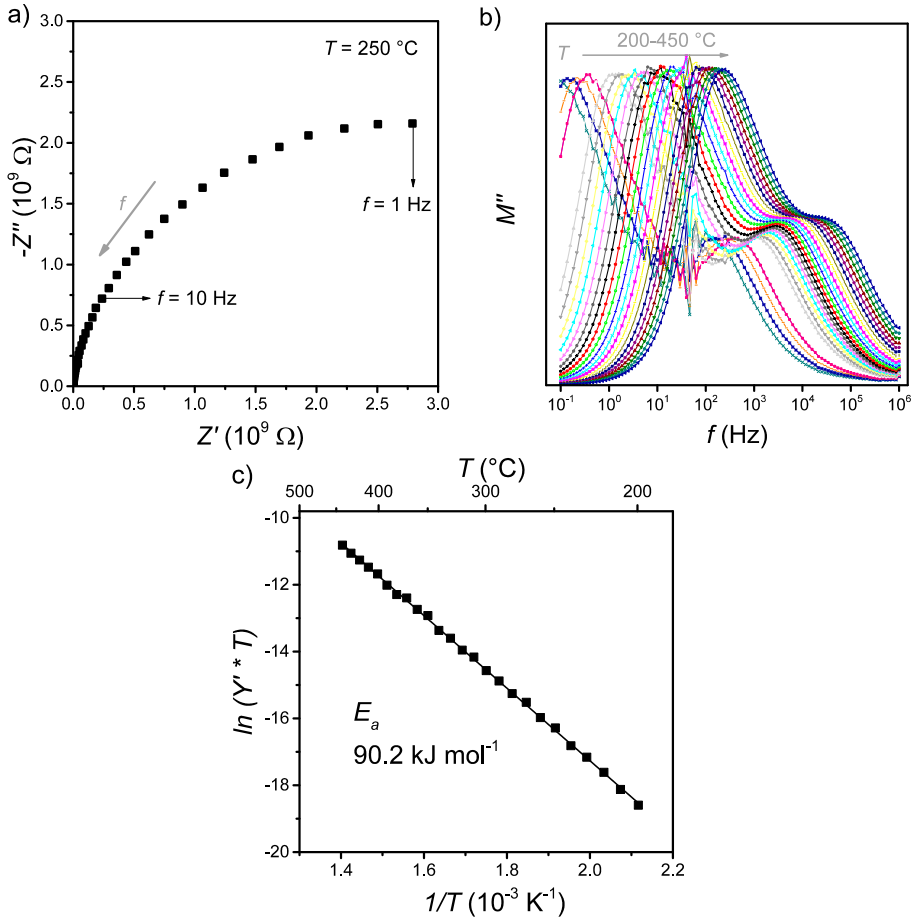

Figure 1. (**a**) Argand diagram (plot of the imaginary part of the impedance $-Z''$ versus the real part of the impedance Z' in the complex plane) of dehydrated H-ZSM-5 (Si/Al 13.5) at 250 °C; the **gray** arrow indicates the increase of frequency; (**b**) modulus spectra of the imaginary part M'' versus frequency f of H-ZSM-5 at temperatures 200–450 °C; the **gray** arrow indicates the increase of temperature; (**c**) Arrhenius-like plot of logarithmic proton conductivity at resonance frequencies (in low-frequency range) derived from the Modulus spectra in (**b**). Reproduced with permission from [29]. The Royal Society of Chemistry, 2016.

The long-range proton transport within the zeolites is temperature-dependent, and can be represented using the Arrhenius equation:

$$\ln(Y' \times T) \sim \ln(\sigma_T) = A - E_a/(k_B \times T), \quad (7)$$

where Y' is the real part of the admittance, i.e., $Y(\omega) = 1/Z(\omega)$, at the resonance frequency f_{res} (determined according to the low-frequency maximum in the Modulus plot at the respective temperature), A is the pre-exponential factor (which depends on the charge and number of the mobile species, its on-site oscillation frequency and the hopping distance [38]), E_a is the activation energy of the proton transport process, σ is the specific conductivity of the zeolite, k_B is the Boltzmann constant, and T is the temperature. An example is shown in Figure 1c for an Arrhenius-like representation of IS results over the zeolite H-ZSM-5.

2.2. Instruments for In Situ IS and In Situ IS-DRIFTS

The measurement configurations for in situ IS and in situ IS-DRIFTS are schematically displayed in Figure 2a,b, respectively. For both methods, the zeolite catalysts were deposited as a thick film on screen-printed interdigital electrodes (IDEs) comprised of an alumina substrate with gold electrodes on the front side and an integrated heater on the reverse side. In this way, an excellent electrical contact between the zeolite film and the IDE structure can be achieved [30]. An external power supply is used for temperature control via resistive heating. Temperature calibration was performed for each sample with a pyrometer for the remote monitoring of temperature on the surface of zeolite film. The gas composition is controlled by mass flow controllers (MFCs) dosing different gases such as NO, O_2, NH_3 and N_2 (carrier gas). Prior to each measurement, the zeolite sample was pretreated at high temperatures (usually at 400 °C in 10 vol. % O_2 for 1 h) to remove any adsorbed water or hydrocarbon contaminants. The electrical impedance of the sample is measured with an impedance analyzer range up to 10^{14} Ω (±1%). The voltage is set to 0.1 V (rms) for all measurements to stay in the linear response regime.

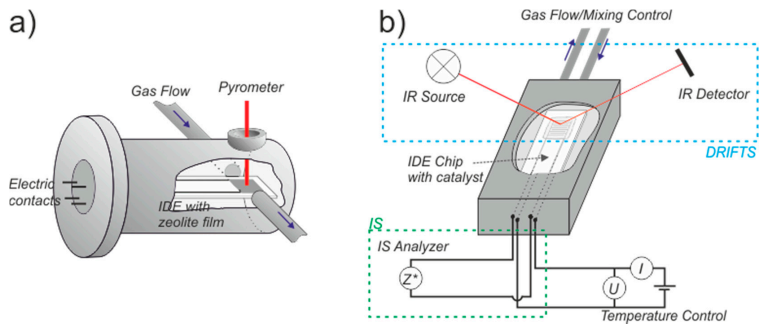

Figure 2. Schematic illustrations of the measurement configurations for (**a**) in situ impedance spectroscopy (IS) and (**b**) in situ IS and diffuse reflection infrared Fourier transformation spectroscopy (in situ IS-DRIFTS). (**a**) Reproduced with permission from [30]; (**b**) adapted with permission from [28], Elsevier, 2016.

The in situ IS measurements were carried out using a homemade reaction chamber (Figure 2a). For in situ IS-DRIFTS measurements, a commercial high-temperature reaction chamber (Harrick Scientific Products, Pleasantville, NY, USA) was modified to allow the introduction of IDE chips with zeolite catalyst film (Figure 2b). A specially designed holder with electrical contacts was employed to keep the sensor chip inside the reaction chamber in a way that the zeolite film is in the focal point of the infrared beam of the DRIFTS mirror design. Simultaneous IS and DRIFTS measurements were carried out using the same catalyst film, allowing simultaneous monitoring of both the proton conductivity of zeolite catalysts and the vibration modes of the molecules on zeolite catalysts [26,28].

3. Proton Transport in Zeolite Catalysts for NH_3-SCR

3.1. NH_3-Supported Proton Transport

Zeolites are a class of crystalline, microporous solids consisting of tetrahedral TO_4 (T denotes as Si, Al, Ti, etc.) units. The TO_4 units serve as primary building blocks forming three-dimensional frameworks with interconnected cages and channels of distinct sizes and shapes. The Brønsted acidity of zeolites, which results from the non-equivalent substitution of T-atoms (e.g., the substitution of Si by Al in TO_4 units as shown in Figure 3) and the subsequent charge-balancing by external, exchangeable cations (Na^+, NH_4^+, H^+, etc.) at the adjacent oxygen sites within the pore space, enables several characteristic functions, such as ion-exchange capacity, proton donating ability and ionic conductivity [3,40–42]. These properties allow zeolites to be used as adsorbents, separators, ionic conductors, sensors, or catalysts [3,40–42].

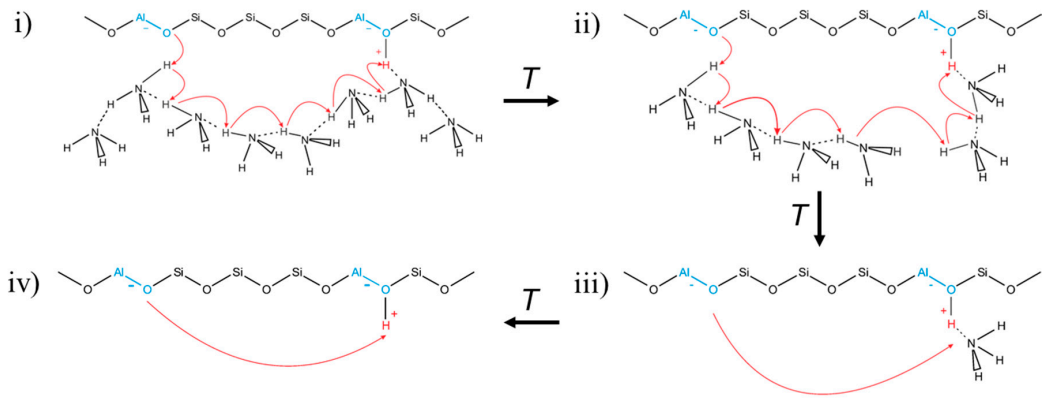

Figure 3. Schematic illustration of the mechanisms of proton transport occurring in NH_3-loaded H-form zeolites at different temperature ranges. (**i**) Grothuss-like proton transport along condensed NH_3 molecules, i.e., $NH_4^+ \cdot (NH_3)_n$ chains (below 120 °C); (**ii**) proton transport along dis-integrated $NH_4^+ \cdot (NH_3)_n$ chains (120–200 °C); (**iii**) vehicle transport mechanism, where NH_4^+ serves as "vehicle" like proton carrier (200–340 °C); and (**iv**) hopping transport of protons by thermal activation (above 340 °C). Adapted with permission from [31]. Copyright American Chemical Society, 2016.

In NH_3-SCR catalysis, protons on Brønsted acid sites of zeolite catalysts could transfer to adsorbed NH_3 forming ammonium ions (NH_4^+), which interact further with NH_3 molecules leading to the formation of $NH_4^+ \cdot (NH_3)_n$ complexes at low temperatures [2]. Both NH_4^+ and $NH_4^+ \cdot (NH_3)_n$ complexes can provide additional paths or carriers for proton transport, which consequently increase the proton conductivity of zeolite catalysts [26,32–34]. The physico-chemical features of NH_3-supported proton transport were revealed by in situ studies over NH_3-loaded zeolites using techniques combining IS with TPD or quantum chemical calculations [26–29,34,43], and are schematically illustrated in Figure 3 for proton-form zeolites. Four distinct temperature-dependent mechanisms can be distinguished, specifically (i) the Grothuss-like transport along condensed $NH_4^+ \cdot (NH_3)_n$ chains at low temperatures, i.e., below the desorption temperature of NH_3; (ii) proton hopping along partially disintegrated chains of NH_3 molecules (i.e., in the temperature range, where weakly bound solvent molecules desorb); (iii) vehicle-supported transfer of protons between the neighboring Brønsted sites with NH_4^+ carriers as "proton vehicles"; and (iv) thermally activated proton hopping along the electron density located at the oxygen atoms of the zeolite lattice in the absence of solvate molecules (above 340 °C) [26,32,33].

3.2. Factors Influencing the Proton Transport in Zeolite Catalysts

As can be seen in Figure 3, the proton transport in zeolites is largely determined by the abundance of Brønsted sites serving as the primary sites for the adsorption of NH_3. This was already confirmed

by our previous studies over ZSM-5 zeolites with different Si/Al ratios [32,33]. For metal-exchanged zeolites used as catalysts in NH_3-SCR, several structural or chemical parameters such as framework topology, metal cation type, and metal exchange level also influence considerably the NH_3-supported proton transport by affecting the formation of $NH_4^+ \cdot (NH_3)_n$ complexes and/or the affinity between the NH_3 species and the zeolite catalysts.

3.2.1. Metal Cation Type

Based on the NH_3-supported proton transport, the loading and desorption of NH_3 in Fe- and Cu-ZSM-5 can be effectively monitored by means of in situ IS (Figure 4a). Comparative studies revealed that, as compared to Fe-ZSM-5, the Cu-ZSM-5 demonstrated a stronger retention ability against thermal desorption for the adsorbed NH_3 species (i.e., NH_4^+ on Brønsted as indicated by the IR band at 1457 cm^{-1}, and the NH_3 on metal sites as indicated by the IR band at 1276/1266 cm^{-1}), which is due to a stronger NH_3-zeolite interaction (according to the higher activation energy E_a for proton transport by multi-frequency IS experiments; see Figure 4b). During exposure in NO/O_2 mixture for the SCR conversion of stored NH_3 (Figure 5), while the proton conductivity of NH_3-saturated Fe-ZSM-5 decreased rapidly, that of NH_3-saturated Cu-ZSM-5 increased further significantly (Figure 5a). Such unexpected increase of proton conductivity during NO/O_2 exposure was observed in the temperature range of 100–250 °C over NH_3-saturated Cu-ZSM-5 (Figure 6a). In situ IS-DRIFTS studies revealed that the increased proton conductivity results mainly from NH_4^+ intermediates (Figure 6b), which formed via the following route: (i) interaction of NO and adsorbed NH_3 on Cu^{2+} sites; (ii) reduction of Cu^{2+} to Cu^+ and release of a proton on the adjacent Brønsted site (i.e., $Cu^{2+} \rightarrow Cu^+ + H^+$); and (iii) interaction of the released proton and adsorbed NH_3 on Cu sites (i.e., $H^+ + NH_3 \rightarrow NH_4^+$) [27,29,44,45]. The enhanced proton transport of NH_3-saturated zeolite catalysts by NO exposure is thus considered to manifest the NO activation ability in the presence of adsorbed NH_3 [29].

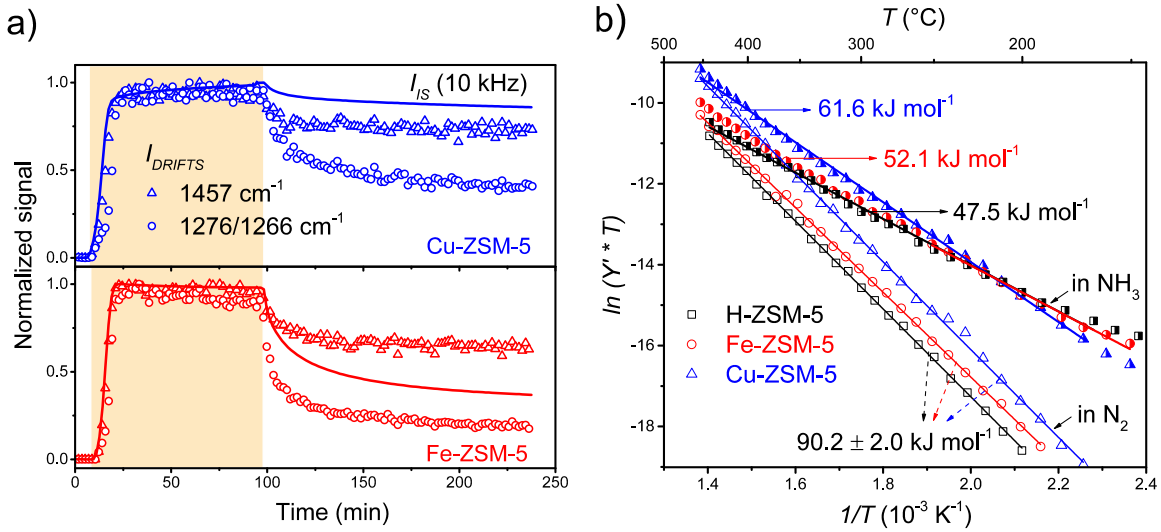

Figure 4. (**a**) simultaneously measured proton conductivity (I_{IS}; IS signal at 10 kHz; solid lines) and DRIFTS signals after Kubelka-Munk (KM) transformation (I_{DRIFTS}; symbols) during the loading and thermal desorption of NH_3 over zeolites at 100 °C. The colorful background indicates the period with NH_3 supply to the system. I_{DRIFTS} at 1457 cm^{-1} (triangles) and 1276/1266 cm^{-1} (circles) are attributed to the bending vibrations of NH_4^+ ions on Brønsted acid sites and bending vibrations of NH_3 species on metal sites, respectively; and (**b**) Arrhenius-like representations for the IS results obtained in flowing N_2 (empty symbols) and NH_3 (100 ppm in N_2; half-filled symbols) over H-ZSM-5 (squares), Fe-ZSM-5 (circles) and Cu-ZSM-5 (triangles). Reproduced with permission from [29]. Copyright The Royal Society of Chemistry, 2016.

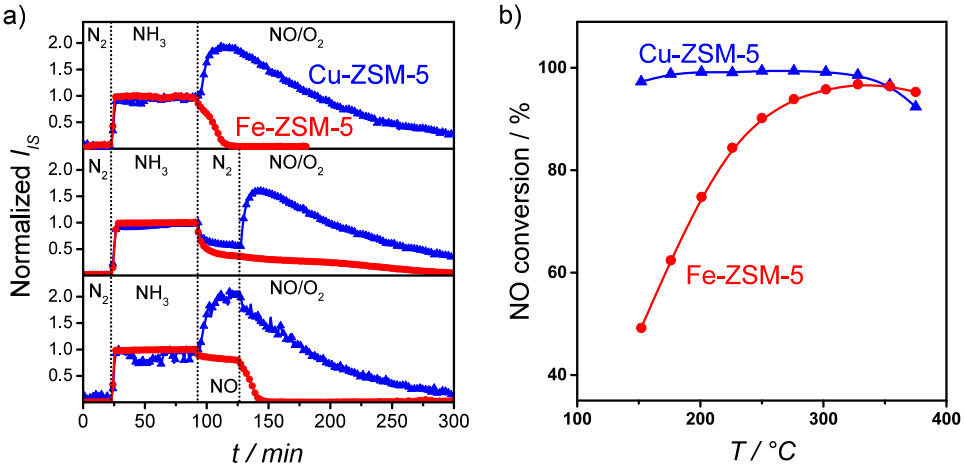

Figure 5. (**a**) time-courses of normalized proton conductivity I_{IS} (at 10 kHz) for Fe-ZSM-5 and Cu-ZSM-5 during exposure to the indicated atmospheres at 175 °C; (**b**) measured NO conversion in selective catalytic reduction (NH_3-SCR) over Fe-ZSM-5 and Cu-ZSM-5 (0.5 g catalyst; a total flow rate of 1 L·min^{-1}; 500 ppm NH_3, 500 ppm NO, 10% O_2, 2% H_2O). Reproduced with permission from [29]. Copyright The Royal Society of Chemistry, 2016.

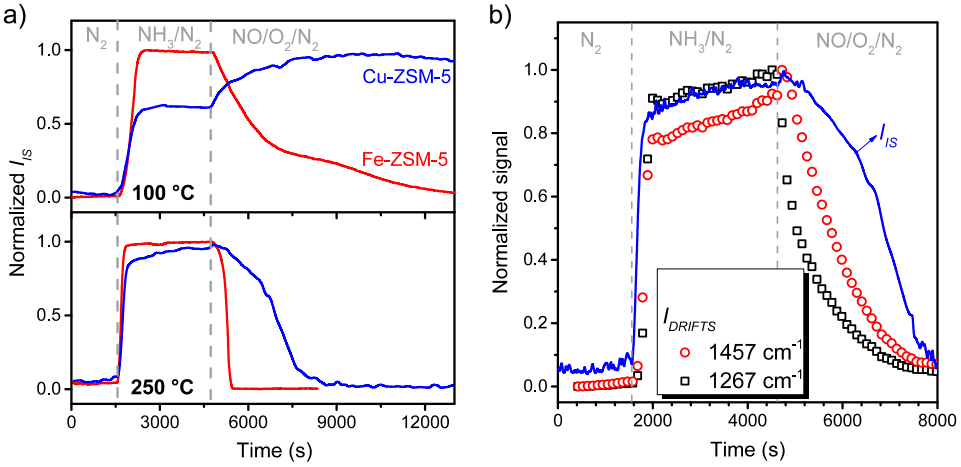

Figure 6. (**a**) time-courses of normalized proton conductivity I_{IS} (at 10 kHz) for Fe-ZSM-5 and Cu-ZSM-5 during exposure to the indicated atmospheres at 100 °C and 250 °C; (**b**) normalized I_{IS} (line) and I_{DRIFTS} signals (symbols) for Cu-ZSM-5 under SCR-related atmospheres at 250 °C. (**a**) Reproduced with permission from [29]. Copyright The Royal Society of Chemistry, 2016; (**b**) Reprinted with permission from [31]. Copyright American Chemical Society, 2016.

It has to be noted that the redox cycle of active metal sites consists of a reduction half-cycle ($Cu^{2+} \rightarrow Cu^{+}$ or $Fe^{3+} \rightarrow Fe^{2+}$) and a re-oxidation half-cycle ($Cu^{+} \rightarrow Cu^{2+}$ or $Fe^{2+} \rightarrow Fe^{3+}$), and the latter one is usually considered to be the rate-determining step in the whole redox processes [10,11]. Therefore, further IS studies on the re-oxidation half-cycle are needed to understand in more detail the very different low-temperature NH_3-SCR activities of Cu- and Fe-exchanged zeolite catalysts (Figure 5b) [29].

3.2.2. Metal Exchange Level

The metal exchange level (estimated according to, for example, the metal to Al ratio in metal-exchange aluminosilicate zeolites) of zeolite catalyst is known to have a strong impact in NH_3-SCR catalysis [46–50]. In the case of ZSM-5 with a Si/Al ratio of 13.5, while the Cu species in

Cu-ZSM-5 remain mainly in isolated state at a Cu/Al ratio of ca. 0.2, a considerable amount of Fe dimers or oligomers form in Fe-ZSM-5 with a Fe/Al ratio of ca. 0.2 and above [31]. The introduced metal species can adsorb NH_3 at an intermediate strength (stronger than the adsorption on Lewis sites, but weaker than that on Brønsted sites), as characterized by the NH_3 desorption at temperatures between 130 and 250 °C (Figure 7a) [7]. The influence of metal exchange level on the NH_3-zeolite interaction can be examined by analyzing the mobility of adsorbed NH_3-species as proton carriers under thermal desorption conditions by means of in situ IS [31]. As indicated by the activation energies for proton transport (i.e., the strength of NH_3 adsorption on zeolites), while the increase of Fe loading weakened slightly the NH_3-zeolite interaction, a higher Cu loading enhanced significantly the NH_3-zeolite interaction (Figure 7b). The weakening interaction between NH_3 and Fe-ZSM-5 with increasing Fe/Al ratio can be clearly visualized in DRIFTS (Figure 7c), according to the decreasing band intensity at 1266 cm^{-1} originating from the NH_3 species on Fe sites [17,31]. In NH_3-SCR catalysis, for the zeolite catalysts shown in Figure 7b, while the low-temperature (below 250 °C) NH_3-SCR activity of Fe-ZSM-5 decreased with Fe/Al ratio, that of Cu-ZSM-5 increased with Cu/Al ratio [17,31].

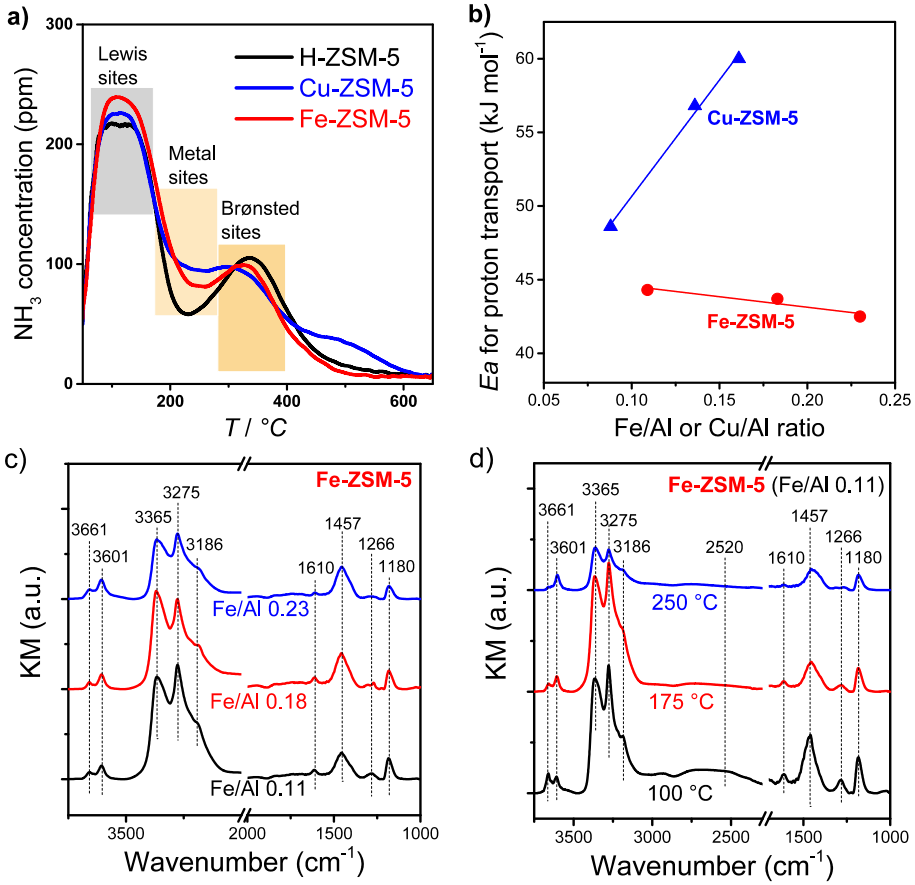

Figure 7. (**a**) NH_3-TPD (temperature-programmed desorption using NH_3 as a probe molecule) profiles showing the desorption of NH_3 species on Lewis sites, metal sites and Brønsted sites in different temperature ranges; (**b**) activation energy (E_a) for proton transport as a function of metal exchange level. The E_a values were derived from the Arrhenius plots of the in situ IS results over NH_3-loaded zeolite catalysts under thermal desorption conditions (in N_2) at temperatures 130–250 °C; (**c**) in situ DRIFT spectra for NH_3-saturated Fe-ZSM-5 zeolite catalysts with different Fe/Al ratios at 175 °C; (**d**) in situ DRIFT spectra for a NH_3-saturated Fe-ZSM-5 zeolite catalyst (Fe/Al ratio of 0.11) at different temperatures. (**a**) Reproduced with permission from [29]. Copyright The Royal Society of Chemistry, 2016; (**b**) Reprinted with permission from [31], American Chemical Society, 2016; (**c**,**d**) Reprinted with permission from [17]. Copyright American Chemical Society, 2016.

At high Fe loadings or under harsh conditions (e.g., hydrothermal aging), the Fe species in Fe-zeolites may aggregate forming Fe_xO_y dimers or small clusters within the zeolite pores, or even relatively large Fe_2O_3 particles outside the zeolite pores [31]. At low temperatures, these Fe_xO_y species or Fe_2O_3 particles could provide additional acidic sites for the adsorption of NH_3 species, favoring the formation of $NH_4^+ \cdot (NH_3)_n$ chains (as indicated by the broad band centered at ca. 2520 cm^{-1} in the DRIFT spectra in Figure 7d) and consequently the proton transport within the zeolite lattice [28,29]. At high temperatures (175 °C and above), however, the weakly bound NH_3 species cannot be retained on the Fe_xO_y species or Fe_2O_3 particles (as indicated by the disappearance of the broad band centered at ca. 2520 cm^{-1}) and thus have no (or just negligible) contribution to the proton transport [17,29].

3.2.3. Zeolite Framework Type

Among different zeolite framework types, those with medium or small pore diameters (such as CHA, MFI, MOR, FER, etc.) after metal ion exchange were found to be especially advantageous for NH_3-SCR catalysis [2–4]. A comparison of Cu-ZSM-5 (MFI type) and Cu-SAPO-34 (CHA type) zeolites using in situ IS revealed that the framework type influenced significantly the proton transport properties of Cu-zeolite catalysts under NH_3-SCR related conditions [27]. At low temperatures, formation of highly proton-conducting NH_4^+ intermediates was observed in both zeolites (Figures 6b and 8), which is due to the reduction of Cu^{2+} to Cu^+ as a result of the interaction of NH_3 and NO [17,25,29,44]. In the monitoring of NH_3-SCR using the zeolite catalysts directly as sensors, while the performance of Cu-SAPO-34 can be improved by increasing the temperature to 200 °C and above, that of Cu-ZSM-5 was impeded by the formation of NH_4^+ intermediates even at high temperatures as 350 °C (Figure 9). Both zeolites performed similarly in the direct monitoring of NH_3-SCR at temperatures above 350 °C. At 200 °C and below, Cu-SAPO-34 also showed higher NH_3-SCR activity than Cu-ZSM-5 [27]. The difference in proton transport, NH_3-SCR reaction monitoring and NH_3-SCR catalysis can be attributed to the different coordinative nature of the metal sites in the two catalysts [4]. Systematic investigations are required to gain more insights into this issue.

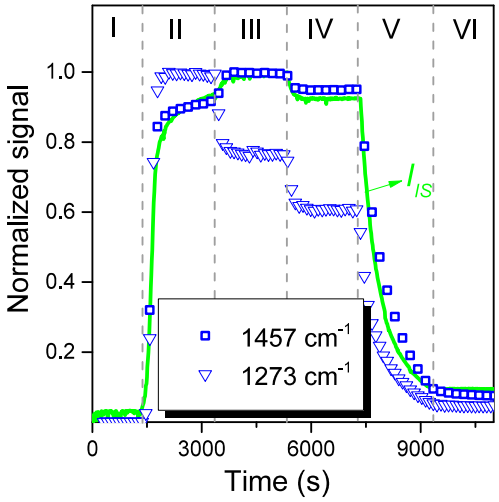

Figure 8. Normalized I_{IS} and I_{DRIFTS} signals obtained over Cu-SAPO-34 at 250 °C in different gas mixtures; (**I**) pure N_2; (**II**) 100 ppm NH_3, N_2 balance; (**III**) 70 ppm NH_3, 20 ppm NO, 10% O_2, N_2 balance; (**IV**) 45 ppm NH_3, 45 ppm NO, 10% O_2, N_2 balance; (**V**) 20 ppm NH_3, 70 ppm NO, 10% O_2, N_2 balance; (**VI**) 100 ppm NO, N_2 balance. Cu-SAPO-34: 1 wt % Cu, (P + Al)/Si = 12.9. 1457 cm^{-1}: NH_4^+ ions on Brønsted acid sites; 1273 cm^{-1}: NH_3 species on Cu sites. Reproduced with permission from [25].

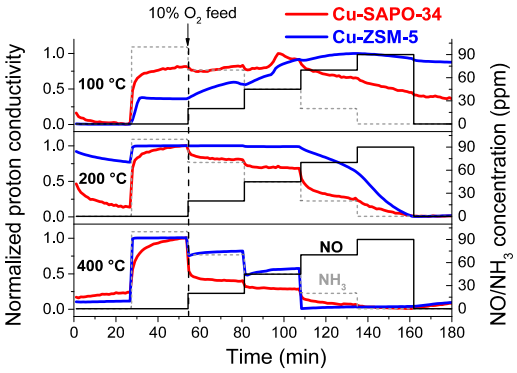

Figure 9. Electric signals of Cu-ZSM-5 and Cu-SAPO-34 in SCR-related atmospheres. Cu-SAPO-34: 1 wt % Cu, (P + Al)/Si = 12.9. Cu-ZSM-5: 1 wt % Cu, Si/Al = 13.5. Reproduced with permission from [27]. Copyright Elsevier, 2016.

3.2.4. Formation of NH_4^+ Intermediates

In zeolite catalyzed NH_3-SCR reactions, depending on the used catalysts and reaction conditions, different intermediate species, such as NO^+ [51], NO_3^- [45], NO_2^- [52], H^+ [11], NH_4^+ [44], have been observed forming. As shown in Figures 6b and 8, highly mobile NH_4^+ intermediates formed on Cu-ZSM-5 and Cu-SAPO-34 as a result of the NH_3-NO interaction [44]. In case of Fe-ZSM-5, due to the well-known NH_3-inhibition effect [10,53], formation of NH_4^+ intermediates (resulting from the reduction of Fe^{3+} to Fe^{2+} similar as the Cu redox cycle) at low reaction temperatures can only be clearly observed by in situ IS-DRIFTS after a partial desorption of adsorbed NH_3 (Figure 10a) [17]. Nevertheless, adsorption and activation of NO did take place on NH_3-satured Fe-ZSM-5, leading to the formation of NH_4^+ intermediates, clearly enhancing the proton conductivity of NH_3-loaded Fe-ZSM-5 in NO (see the higher I_{IS} values during exposure in NO than in N_2; Figure 10b). These observations indicate a $Fe^{3+} \leftrightarrow Fe^{2+}$ redox cycle in Fe-ZSM-5 catalysts similar as the widely accepted $Cu^{2+} \leftrightarrow Cu^+$ redox cycle in Cu-SSZ-13 catalysts (Figure 11a) [3,10,11,44,45,54]. More interestingly, the formed NH_4^+ intermediates were found to largely determine the NH_3-SCR activity of Fe-ZSM-5 catalysts at low temperatures (Figure 11b). Therefore, the formation of NH_4^+ intermediates, indicating the activation of NO in the presence of adsorbed NH_3, may potentially serve as a 'descriptor' of the activity of Fe-zeolite catalyst for NH_3-SCR, especially at low temperatures.

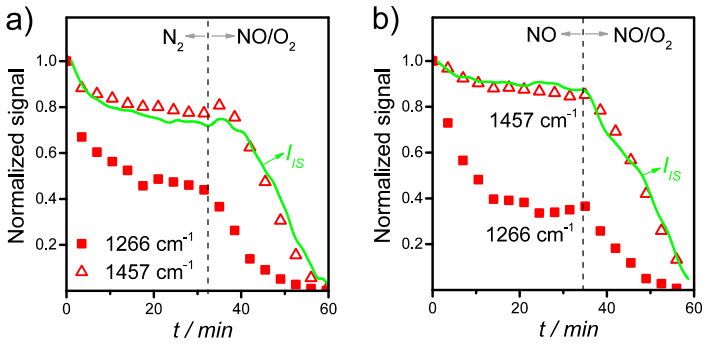

Figure 10. Normalized I_{IS} (**green** line) and DRIFTS signals (**red** symbols) at characteristic wavenumbers of NH_3-loaded Fe-ZSM-5 (Si/Al 13.5, Fe/Al 0.11) exposed N_2 and NO/O_2 mixture in sequence (**a**) and exposed to NO and NO/O_2 mixture in sequence (**b**). I_{IS}: absolute value of complex admittance $|Y^*|$ (Y^* is the reciprocal of the complex impedance Z^*, i.e., $Y^* = 1/Z^*$) at 10 kHz. 1457 cm^{-1}: NH_4^+ ions on Brønsted acid sites; 1266 cm^{-1}: NH_3 species on Fe sites. The catalyst was pre-treated at 450 °C in 10% O_2 for 1 h before each measurement. Reprinted with permission from [17]. Copyright American Chemical Society, 2016.

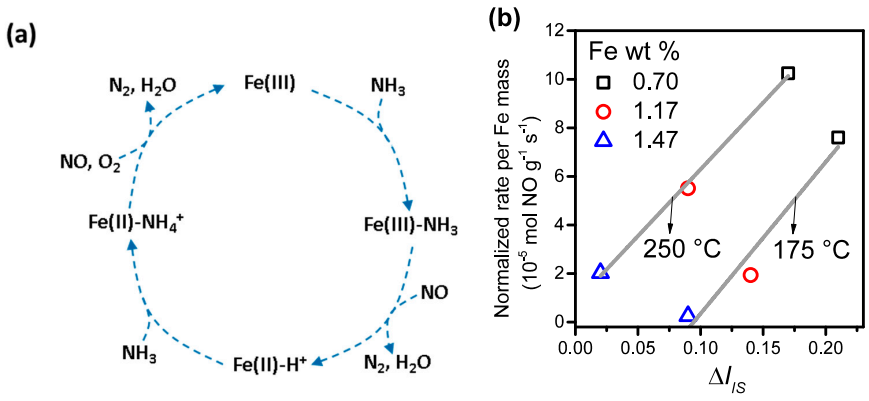

Figure 11. (**a**) proposed pathway for the formation of NH_4^+ intermediate in NH_3-SCR over Fe-ZSM-5 catalysts; (**b**) correlation between the NH_4^+ intermediate formation and the normalized NO reduction rates at low temperatures; the NH_4^+ intermediate formation (ΔI_{IS}) was evaluated according to the proton conductivity enhancement of NH_3-loaded Fe-ZSM-5 after exposure in NO for 30 min in comparison to exposure in N_2 for 30 min. Reprinted with permission from [17]. Copyright American Chemical Society, 2016.

3.2.5. H_2O Vapor

In real diesel exhausts, a considerable amount of H_2O vapor resulting from the fuel combustion processes and the NH_3-SCR reactions is always present. As revealed previously, H_2O as a solvate molecule could serve as proton carrier as well and consequently enhance the proton conductivity of zeolites in a broad temperature range [33]. As compared to NH_3, H_2O demonstrates a significantly weaker supporting effect for the proton transport in zeolites [16], specifically, 1 vol. % H_2O vapor only has the same effect as 6 ppm of NH_3 in terms of the conductivity change of H-ZSM-5 (at 420 °C) [55]. In the above-mentioned transient IS measurements (in the absence of H_2O), a significant influence of H_2O as the product of NH_3-SCR reaction can thus be ruled out because of the very low concentration. Nevertheless, minor contribution of H_2O to the overall proton conductivity of the respective zeolite catalyst cannot be fully excluded. Further comparative studies (with or without H_2O) are required to achieve a more complete understanding of the influence of H_2O.

3.2.6. Zeolite Crystallite Size

Although the crystallite size of zeolite was found to influence limitedly the intrinsic NH_3-SCR activities of metal-exchanged zeolite catalysts (e.g., Cu-SSZ-13, Cu-SAPO-34, Fe-ZSM-5) [56–58], a decrease of crystal size from several micrometers to 50–100 nm can improve the hydrothermal stability of zeolite catalysts [56,57]. For proton transport in zeolites, the influence of crystallite size (or grain boundary) is negligible with crystallite size at micrometer level, and is noted only with crystallite sizes below 200 nm [59]. Considering that commercially relevant zeolite materials with a broad distribution of crystallite size (0.5–5 μm) were applied in the above-mentioned IS studies [17,25–36], a noticeable influence of the zeolite crystallite size can be excluded.

4. Summary and Perspectives

In summary, by analyzing the proton transport properties of zeolite catalysts under SCR-related reaction conditions using in situ IS, the NH_3-zeolite interaction, NO-zeolite interaction (in the presence of adsorbed NH_3), and formation of proton-conducting intermediates can be probed. A combination of IS with DRIFTS allows for understanding molecularly the proton transport properties of zeolite NH_3-SCR catalysts. Several structural or chemical parameters, such as framework topology, metal cation type and metal exchange level, influenced the proton transport to different degrees by affecting the reactant–zeolite interactions. On the one hand, the mobility of adsorbed NH_3-species as proton

carriers, determined by the NH_3-zeolite interaction, was influenced differently by the type, loading and coordinative environment of the exchanged Fe or Cu species in zeolite catalysts. On the other hand, highly mobile NH_4^+ intermediates, as identified by IS combined with DRIFTS, can form on zeolite catalysts as general intermediate species resulting from the interaction of co-adsorbed NH_3 and NO on metal active sites. The formed NH_4^+ intermediates not only significantly influenced the proton transport properties, and consequently the reaction monitoring performance of zeolite catalysts due to the highly proton-conducting nature, but also largely determined the low-temperature NH_3-SCR activity because of their high mobility and reactivity. These findings, which are not easily achievable by conventional methods, thus provide new perspectives to understand mechanistically the NH_3-SCR reaction over zeolite catalysts.

To understand further the role of proton transport in NH_3-SCR catalysis, both chemical nature (e.g., surface acidity, chemical composition) and structural properties (e.g., size, shape, or porosity) of the zeolite catalysts should be taken into account. Substantial improvements, for example the synthesis of zeolites with well-controlled crystal sizes or porosity, have already been achieved using delicately designed bottom-up (i.e., controlling the chemical and structural properties by adjusting the synthetic procedure) or top–down (i.e., post-synthetic modifications) approaches [60,61]. Although the electrical and catalytic properties of zeolites can be correlated to certain specific chemical or structural features in a collective manner, it is still practically challenging to discriminate intrinsic and interfacial effects in the mentioned applications. In recent years, several advanced techniques, such as X-ray based micro-spectroscopy or local-probe measurement, have been developed to analyze in situ the chemical nature, the three-dimensional structure, the electrical properties, and eventually the structure–activity relationship at single-particle levels without the interference of boundary effects [15,62,63]. It is expected that a combination of these new techniques will promote achieving more reliable guidelines for the rational development of zeolite catalysts in the future.

Acknowledgments: We appreciate the funding from the German Research Foundation (DFG) under grant SI 609/14-1, and from the Exploratory Research Space of RWTH Aachen University financed by the Excellence Initiative of the German federal and state governments to promote science and research at German universities.

Author Contributions: P.C. and U.S. wrote the draft and improved the manuscript based on the reviewers' comments.

Conflicts of Interest: The authors declare no conflict of interest.

References

1. Granger, P.; Parvulescu, V.I. Catalytic NO_x Abatement Systems for Mobile Sources: From Three-Way to Lean Burn after-Treatment Technologies. *Chem. Rev.* **2011**, *111*, 3155–3207. [CrossRef] [PubMed]
2. Brandenberger, S.; Kröcher, O.; Tissler, A.; Althoff, R. The State of the Art in Selective Catalytic Reduction of NO_x by Ammonia Using Metal-Exchanged Zeolite Catalysts. *Catal. Rev.* **2008**, *50*, 492–531. [CrossRef]
3. Beale, A.M.; Gao, F.; Lezcano-Gonzalez, I.; Peden, C.H.F.; Szanyi, J. Recent Advances in Automotive Catalysis for NO_x Emission Control by Small-Pore Microporous Materials. *Chem. Soc. Rev.* **2015**, *44*, 7371–7405. [CrossRef] [PubMed]
4. Deka, U.; Lezcano-Gonzalez, I.; Weckhuysen, B.M.; Beale, A.M. Local Environment and Nature of Cu Active Sites in Zeolite-Based Catalysts for the Selective Catalytic Reduction of NO_x. *ACS Catal.* **2013**, *3*, 413–427. [CrossRef]
5. Yu, T.; Hao, T.; Fan, D.; Wang, J.; Shen, M.; Li, W. Recent NH_3-SCR Mechanism Research over Cu/SAPO-34 Catalyst. *J. Phys. Chem. C* **2014**, *118*, 6565–6575. [CrossRef]
6. Li, Y.; Deng, J.; Song, W.; Liu, J.; Zhao, Z.; Gao, M.; Wei, Y.; Zhao, L. Nature of Cu Species in Cu-SAPO-18 Catalyst for NH_3–SCR: Combination of Experiments and DFT Calculations. *J. Phys. Chem. C* **2016**, *120*, 14669–14680. [CrossRef]
7. Lezcano-Gonzalez, I.; Deka, U.; Arstad, B.; Van Yperen-De Deyne, A.; Hemelsoet, K.; Waroquier, M.; Van Speybroeck, V.; Weckhuysen, B.M.; Beale, A.M. Determining the Storage, Availability and Reactivity of NH_3 within Cu-Chabazite-based Ammonia Selective Catalytic Reduction Systems. *Phys. Chem. Chem. Phys.* **2014**, *16*, 1639–1650. [CrossRef] [PubMed]

8. Brandenberger, S.; Kröcher, O.; Wokaun, A.; Tissler, A.; Althoff, R. The Role of Brønsted Acidity in the Selective Catalytic Reduction of NO with Ammonia over Fe-ZSM-5. *J. Catal.* **2009**, *268*, 297–306. [CrossRef]
9. Maier, S.M.; Jentys, A.; Janousch, M.; van Bokhoven, J.A.; Lercher, J.A. Unique Dynamic Changes of Fe Cationic Species under NH_3-SCR Conditions. *J. Phys. Chem. C* **2012**, *116*, 5846–5856. [CrossRef]
10. Boubnov, A.; Carvalho, H.W.; Doronkin, D.E.; Gunter, T.; Gallo, E.; Atkins, A.J.; Jacob, C.R.; Grunwaldt, J.D. Selective Catalytic Reduction of NO over Fe-ZSM-5: Mechanistic Insights by Operando HERFD-XANES and Valence-to-core X-ray Emission Spectroscopy. *J. Am. Chem. Soc.* **2014**, *136*, 13006–13015. [CrossRef] [PubMed]
11. Paolucci, C.; Parekh, A.A.; Khurana, I.; Di Iorio, J.R.; Li, H.; Albarracin Caballero, J.D.; Shih, A.J.; Anggara, T.; Delgass, W.N.; Miller, J.T.; et al. Catalysis in a Cage: Condition-Dependent Speciation and Dynamics of Exchanged Cu Cations in SSZ-13 Zeolites. *J. Am. Chem. Soc.* **2016**, *138*, 6028–6048. [CrossRef] [PubMed]
12. Moreno-González, M.; Hueso, B.; Boronat, M.; Blasco, T.; Corma, A. Ammonia-Containing Species Formed in Cu-Chabazite As Per In Situ EPR, Solid-State NMR, and DFT Calculations. *J. Phys. Chem. Lett.* **2015**, *6*, 1011–1017. [CrossRef] [PubMed]
13. Borfecchia, E.; Lomachenko, K.A.; Giordanino, F.; Falsig, H.; Beato, P.; Soldatov, A.V.; Bordiga, S.; Lamberti, C. Revisiting the Nature of Cu Sites in the Activated Cu-SSZ-13 Catalyst for SCR Reaction. *Chem. Sci.* **2015**, *6*, 548–563. [CrossRef]
14. Svelle, S.; Tuma, C.; Rozanska, X.; Kerber, T.; Sauer, J. Quantum Chemical Modeling of Zeolite-catalyzed Methylation Reactions: Toward Chemical Accuracy for Barriers. *J. Am. Chem. Soc.* **2009**, *131*, 816–825. [CrossRef] [PubMed]
15. Vogt, E.T.; Weckhuysen, B.M. Fluid Catalytic Cracking: Recent Developments on the Grand Old Lady of Zeolite Catalysis. *Chem. Soc. Rev.* **2015**, *44*, 7342–7370. [CrossRef] [PubMed]
16. Sauer, J. Proton Transfer in Zeolites. In *Hydrogen-Transfer Reactions*; Hynes, J.T., Klinman, J.P., Limbach, H.-H., Schowen, R.L., Eds.; Wiley-VCH: Weinheim, Germany, 2006; pp. 685–707.
17. Chen, P.; Jabłońska, M.; Weide, P.; Caumanns, T.; Weirich, T.; Muhler, M.; Moos, R.; Palkovits, R.; Simon, U. Formation and Effect of NH_4^+ Intermediates in NH_3–SCR over Fe-ZSM-5 Zeolite Catalysts. *ACS Catal.* **2016**, *6*, 7696–7700. [CrossRef]
18. Sierka, M.; Sauer, J. Proton Mobility in Chabazite, Faujasite, and ZSM-5 Zeolite Catalysts, Comparison Based on Ab Initio Calculations. *J. Phys. Chem. B* **2001**, *105*, 1603–1613. [CrossRef]
19. Kanellopoulos, J.; Gottert, C.; Schneider, D.; Knorr, B.; Prager, D.; Ernst, H.; Freude, D. NMR Investigation of Proton Mobility in Zeolites. *J. Catal.* **2008**, *255*, 68–78. [CrossRef]
20. Liu, N.; Chen, B.; Li, Y.; Zhang, R.; Liang, X.; Li, Y.; Lei, Z. Charge Transfer Analysis on the Direct Decomposition of Nitrous Oxide over Fe-BEA Zeolite: An Experimental and Density Functional Study. *J. Phys. Chem. C* **2011**, *115*, 12883–12890. [CrossRef]
21. Huo, H.; Peng, L.; Grey, C.P. Low Temperature ^{1}H MAS NMR Spectroscopy Studies of Proton Motion in Zeolite HZSM-5. *J. Phys. Chem. C* **2009**, *113*, 8211–8219. [CrossRef]
22. Derouane, E.G.; Védrine, J.C.; Pinto, R.R.; Borges, P.M.; Costa, L.; Lemos, M.; Lemos, F.; Ribeiro, F.R. The Acidity of Zeolites: Concepts, Measurements and Relation to Catalysis: A Review on Experimental and Theoretical Methods for the Study of Zeolite Acidity. *Catal. Rev.* **2013**, *55*, 454–515. [CrossRef]
23. Brüggemann, T.C.; Keil, F.J. Theoretical Investigation of the Mechanism of the Oxidation of Nitrogen Oxide on Iron-Form Zeolites in the Presence of Water. *J. Phys. Chem. C* **2011**, *115*, 2114–2133. [CrossRef]
24. Sajith, P.K.; Shiota, Y.; Yoshizawa, K. Role of Acidic Proton in the Decomposition of NO over Dimeric Cu(I) Active Sites in Cu-ZSM-5 Catalyst: A QM/MM Study. *ACS Catal.* **2014**, *4*, 2075–2085. [CrossRef]
25. Chen, P.; Schönebaum, S.; Simons, T.; Rauch, D.; Moos, R.; Simon, U. In Situ Monitoring of DeNO$_x$-SCR on Zeolite Catalysts by Means of Simultaneous Impedance and DRIFT Spectroscopy. *Procedia Eng.* **2015**, *120*, 257–260. [CrossRef]
26. Chen, P.; Schönebaum, S.; Simons, T.; Rauch, D.; Dietrich, M.; Moos, R.; Simon, U. Correlating the Integral Sensing Properties of Zeolites with Molecular Processes by Combining Broadband Impedance and DRIFT Spectroscopy-A New Approach for Bridging the Scales. *Sensors* **2015**, *15*, 28915–28941. [CrossRef] [PubMed]
27. Chen, P.; Simböck, J.; Schönebaum, S.; Rauch, D.; Simons, T.; Palkovits, R.; Moos, R.; Simon, U. Monitoring NH_3 Storage and Conversion in Cu-ZSM-5 and Cu-SAPO-34 Catalysts for NH_3-SCR by Simultaneous Impedance and DRIFT Spectroscopy. *Sens. Actuators B* **2016**, *236*, 1075–1082. [CrossRef]

28. Simons, T.; Chen, P.; Rauch, D.; Moos, R.; Simon, U. Sensing Catalytic Conversion: Simultaneous DRIFT and Impedance Spectroscopy for in Situ Monitoring of NH_3–SCR on Zeolites. *Sens. Actuators B* **2016**, *224*, 492–499. [CrossRef]
29. Chen, P.; Rauch, D.; Weide, P.; Schönebaum, S.; Simons, T.; Muhler, M.; Moos, R.; Simon, U. The Effect of Cu and Fe Cations on NH_3-supported Proton Transport in $DeNO_x$-SCR Zeolite Catalysts. *Catal. Sci. Technol.* **2016**, *6*, 3362–3366. [CrossRef]
30. Simons, T.; Simon, U. Zeolites as Nanoporous, Gas-sensitive Materials for in Situ Monitoring of $DeNO_x$-SCR. *Beilstein J. Nanotechnol.* **2012**, *3*, 667–673. [CrossRef] [PubMed]
31. Chen, P.; Moos, R.; Simon, U. Metal Loading Affects the Proton Transport Properties and the Reaction Monitoring Performance of Fe-ZSM-5 and Cu-ZSM-5 in NH_3-SCR. *J. Phys. Chem. C* **2016**, *120*, 25361–25370. [CrossRef]
32. Franke, M.E.; Simon, U.; Moos, R.; Knezevic, A.; Muller, R.; Plog, C. Development and Working Principle of an Ammonia Gas Sensor Based on a Refined Model for Solvate Supported Proton Transport in Zeolites. *Phys. Chem. Chem. Phys.* **2003**, *5*, 5195–5198. [CrossRef]
33. Franke, M.E.; Simon, U. Solvate-supported Proton Transport in Zeolites. *ChemPhysChem* **2004**, *5*, 465–472. [CrossRef] [PubMed]
34. Rodriguez-Gonzalez, L.; Rodriguez-Castellon, E.; Jimenez-Lopez, A.; Simon, U. Correlation of TPD and Impedance Measurements on the Desorption of NH_3 from Zeolite H-ZSM-5. *Solid State Ion.* **2008**, *179*, 1968–1973. [CrossRef]
35. Rauch, D.; Dietrich, M.; Simons, T.; Simon, U.; Porch, A.; Moos, R. Microwave Cavity Perturbation Studies on H-form and Cu Ion-Exchanged SCR Catalyst Materials: Correlation of Ammonia Storage and Dielectric Properties. *Top. Catal.* **2016**. [CrossRef]
36. Rauch, D.; Kubinski, D.; Simon, U.; Moos, R. Detection of the Ammonia Loading of a Cu Chabazite SCR Catalyst by a Radio Frequency-based Method. *Sens. Actuators B* **2014**, *205*, 88–93. [CrossRef]
37. Barsoukov, E.; Macdonald, J.R. *Impedance Spectroscopy: Theory, Experiment, and Applications*, 2nd ed.; John Wiley & Sons, Inc.: Hoboken, NJ, USA, 2005.
38. Simon, U.; Franke, M.E. Electrical Properties of Nanoscaled Host-guest Compounds. *Microporous Mesoporous Mater.* **2000**, *41*, 1–36. [CrossRef]
39. Simon, U.; Flesch, U. Cation-cation Interaction in Dehydrated Zeolites X and Y Monitored by Modulus Spectroscopy. *J. Porous Mater.* **1999**, *6*, 33–40. [CrossRef]
40. Dragomirova, R.; Wohlrab, S. Zeolite Membranes in Catalysis—From Separate Units to Particle Coatings. *Catalysts* **2015**, *5*, 2161–2222. [CrossRef]
41. Tolle, P.; Kohler, C.; Marschall, R.; Sharifi, M.; Wark, M.; Frauenheim, T. Proton Transport in Functionalised Additives for PEM Fuel Cells: Contributions from Atomistic Simulations. *Chem. Soc. Rev.* **2012**, *41*, 5143–5159. [CrossRef] [PubMed]
42. Zheng, Y.; Li, X.; Dutta, P.K. Exploitation of Unique Properties of Zeolites in the Development of Gas Sensors. *Sensors* **2012**, *12*, 5170–5194. [CrossRef] [PubMed]
43. Rodríguez-González, L.; Simon, U. NH_3-TPD Measurements Using a Zeolite-based Sensor. *Meas. Sci. Technol.* **2010**, *21*, 027003. [CrossRef]
44. Paolucci, C.; Verma, A.A.; Bates, S.A.; Kispersky, V.F.; Miller, J.T.; Gounder, R.; Delgass, W.N.; Ribeiro, F.H.; Schneider, W.F. Isolation of the Copper Redox Steps in the Standard Selective Catalytic Reduction on Cu-SSZ-13. *Angew. Chem. Int. Ed.* **2014**, *53*, 11828–11833. [CrossRef] [PubMed]
45. Janssens, T.V.W.; Falsig, H.; Lundegaard, L.F.; Vennestrøm, P.N.R.; Rasmussen, S.B.; Moses, P.G.; Giordanino, F.; Borfecchia, E.; Lomachenko, K.A.; Lamberti, C.; et al. A Consistent Reaction Scheme for the Selective Catalytic Reduction of Nitrogen Oxides with Ammonia. *ACS Catal.* **2015**, *5*, 2832–2845. [CrossRef]
46. Gao, F.; Zheng, Y.; Kukkadapu, R.K.; Wang, Y.; Walter, E.D.; Schwenzer, B.; Szanyi, J.; Peden, C.H.F. Iron Loading Effects in Fe/SSZ-13 NH_3-SCR Catalysts: Nature of the Fe Ions and Structure–Function Relationships. *ACS Catal.* **2016**, *6*, 2939–2954. [CrossRef]
47. Andonova, S.; Tamm, S.; Montreuil, C.; Lambert, C.; Olsson, L. The Effect of Iron Loading and Hydrothermal Aging on One-pot Synthesized Fe/SAPO-34 for Ammonia SCR. *Appl. Catal. B* **2016**, *180*, 775–787. [CrossRef]
48. Brandenberger, S.; Kröcher, O.; Tissler, A.; Althoff, R. The Determination of the Activities of Different Iron Species in Fe-ZSM-5 for SCR of NO by NH_3. *Appl. Catal. B* **2010**, *95*, 348–357. [CrossRef]

49. Gao, F.; Walter, E.D.; Karp, E.M.; Luo, J.; Tonkyn, R.G.; Kwak, J.H.; Szanyi, J.; Peden, C.H.F. Structure–Activity Relationships in NH_3-SCR over Cu-SSZ-13 as Probed by Reaction Kinetics and EPR Studies. *J. Catal.* **2013**, *300*, 20–29. [CrossRef]
50. Gao, F.; Washton, N.M.; Wang, Y.; Kollár, M.; Szanyi, J.; Peden, C.H.F. Effects of Si/Al Ratio on Cu/SSZ-13 NH_3-SCR Catalysts: Implications for the Active Cu Species and the Roles of Brønsted Acidity. *J. Catal.* **2015**, *331*, 25–38. [CrossRef]
51. Kwak, J.H.; Lee, J.H.; Burton, S.D.; Lipton, A.S.; Peden, C.H.; Szanyi, J. A Common Intermediate for N_2 Formation in Enzymes and Zeolites: Side-on Cu-nitrosyl Complexes. *Angew. Chem. Int. Ed.* **2013**, *52*, 9985–9989. [CrossRef] [PubMed]
52. Ruggeri, M.P.; Selleri, T.; Colombo, M.; Nova, I.; Tronconi, E. Identification of Nitrites/HONO as Primary Products of NO Oxidation over Fe-ZSM-5 and Their Role in the Standard SCR Mechanism: A Chemical Trapping Study. *J. Catal.* **2014**, *311*, 266–270. [CrossRef]
53. Gao, F.; Wang, Y.; Kollár, M.; Washton, N.M.; Szanyi, J.; Peden, C.H.F. A Comparative Kinetics Study between Cu/SSZ-13 and Fe/SSZ-13 SCR Catalysts. *Catal. Today* **2015**, *258*, 347–358. [CrossRef]
54. Gunter, T.; Carvalho, H.W.; Doronkin, D.E.; Sheppard, T.; Glatzel, P.; Atkins, A.J.; Rudolph, J.; Jacob, C.R.; Casapu, M.; Grunwaldt, J.D. Structural Snapshots of the SCR Reaction mechanism on Cu-SSZ-13. *Chem. Commun.* **2015**, *51*, 9227–9230. [CrossRef] [PubMed]
55. Moos, R.; Müller, R.; Plog, C.; Knezevic, A.; Leye, H.; Irion, E.; Braun, T.; Marquardt, K.-J.; Binder, K. Selective Ammonia Exhaust Gas Sensor for Automotive Applications. *Sens. Actuators B* **2002**, *83*, 181–189. [CrossRef]
56. Takata, T.; Tsunoji, N.; Takamitsu, Y.; Sadakane, M.; Sano, T. Nanosized CHA Zeolites with High Thermal and Hydrothermal Stability Derived from the Hydrothermal Conversion of FAU Zeolite. *Microporous Mesoporous Mater.* **2016**, *225*, 524–533. [CrossRef]
57. Hu, X.; Yang, M.; Fan, D.; Qi, G.; Wang, J.; Wang, J.; Yu, T.; Li, W.; Shen, M. The Role of Pore Diffusion in Determining NH_3 SCR Active Sites over Cu/SAPO-34 Catalysts. *J. Catal.* **2016**, *341*, 55–66. [CrossRef]
58. Feng, B.; Wang, Z.; Sun, Y.; Zhang, C.; Tang, S.; Li, X.; Huang, X. Size Controlled ZSM-5 on the Structure and Performance of Fe Catalyst in the Selective Catalytic Reduction of NO_x with NH_3. *Catal. Commun.* **2016**, *80*, 20–23. [CrossRef]
59. Severance, M.; Zheng, Y.; Heck, E.; Dutta, P.K. Influence of Crystallite Size on Cation Conductivity in Faujasitic Zeolites. *J. Phys. Chem. A* **2013**, *117*, 13704–13711. [CrossRef] [PubMed]
60. Mintova, S.; Jaber, M.; Valtchev, V. Nanosized Microporous Crystals: Emerging Applications. *Chem. Soc. Rev.* **2015**, *44*, 7207–7233. [CrossRef] [PubMed]
61. Dapsens, P.Y.; Mondelli, C.; Perez-Ramirez, J. Design of Lewis-acid Centres in Zeolitic Matrices for the Conversion of Renewables. *Chem. Soc. Rev.* **2015**, *44*, 7025–7043. [CrossRef] [PubMed]
62. Buurmans, I.L.; Weckhuysen, B.M. Heterogeneities of Individual Catalyst Particles in Space and Time as Monitored by Spectroscopy. *Nat. Chem.* **2012**, *4*, 873–886. [CrossRef] [PubMed]
63. Saltzmann, T.; Bornhofft, M.; Mayer, J.; Simon, U. Shape without Structure: An Intriguing Formation Mechanism in the Solvothermal Synthesis of the Phase-Change Material Sb_2Te_3. *Angew. Chem. Int. Ed.* **2015**, *54*, 6632–6636. [CrossRef] [PubMed]